Proceedings of the 4th International Conference on Mechatronics and Smart Systems
DOI: 10.54254/2755-2721/2026.33080

Multi-source Fusion Intelligent Compensation System for Online Measurement and Intelligent Compensation of Geometric Errors in Large CNC Machine Tools

Siyi Sun[1], Chenyue Li[1], Xiaojin Guo[1], Ruoxi Han[1], Rui He[1], Qing Zhang[1*]

[1]*School of Artificial Intelligence and Computer Science, North China University of Technology, Beijing, China*
**Corresponding Author. Email: zqicl@ncut.edu.cn*

Abstract. To overcome offline lag, difficult decoupling, poor real-time accuracy & poor adaptability of geometric errors in large CNC long-stroke machining, this paper proposes a multi-source fusion intelligent compensation system. For an XYTZ gantry CNC, it builds a multi-source network (dual-frequency laser interferometer, photoelectric encoder, industrial gyroscope, temperature sensor); based on HTM & multi-body theory, establishes a 21-term geometric error model integrating Abbe & Bryan principles & friction thermal deformation for geometric-thermal coupling; uses adaptive Kalman filtering for real-time multi-source data fusion & error sensitivity matrix for fast spatial error decoupling; and deploys a ROS2-based distributed real-time compensation architecture delivering ms-level compensation via FANUC's EPO interface synchronized with the interpolation cycle. Theory & design show: over 5m stroke, compensation accuracy >±10 μm, delay ≤1.5 ms, solving weak real-time & poor robustness, thus supporting precision large-CNC machining.

Keywords: Large CNC machine tools, Geometric errors, Multi-source information fusion, Online measurement, Intelligent compensation

1. Introduction

Demand for large complex parts in aerospace, rail transit, and energy equipment drives CNC machines toward long stroke, high precision, and high dynamics. For large gantry CNCs (>5 m stroke), spatial error >200 μm, thermal error >40%, limiting precision—a key bottleneck [1].

Current offline compensation (laser interferometer, tracker, ballbar with lookup tables) fails for long-stroke dynamics: offline lag misses thermal drift/load deformation; single-source lacks robustness; HTM models omit Abbe/Bryan principles, limiting decoupling; third-party systems >10 ms delay mismatches CNC cycles, degrading high-speed compensation [2]. Multi-sensor fusion and deep learning offer promise, but weak adaptive fusion, lagging prediction, poor integration persist—no high-accuracy, low-latency, robust closed-loop solution exists.

This paper proposes a multi-source fusion online measurement and intelligent compensation system for large CNC geometric errors. For an XYTZ gantry CNC, it builds a multi-source network (dual-frequency laser interferometer [3], absolute encoder, gyroscope, temperature sensor);

© 2026 The Authors. This is an open access article distributed under the terms of the Creative Commons Attribution License 4.0 (https://creativecommons.org/licenses/by/4.0/).

DOI: 10.54254/2755-2721/2026.33080

establishes a geometric-thermal coupled 21-error model integrating Abbe, Bryan, and friction thermal deformation [4,5]; uses adaptive Kalman filtering [6,7] for real-time fusion, plus sensitivity matrix and weighted least squares for fast decoupling [8]; designs LSTM-based ahead-of-time prediction [9]; and deploys ROS2 real-time architecture, delivering ms-level compensation via FANUC's EPO interface synchronized with the interpolation cycle. Expected results: over 5 m stroke, compensation accuracy >±10 μm, delay ≤1.5 ms—a viable solution for high-precision large CNC machining.

2. System overall architecture

The system uses a "sensing–computing–execution" closed-loop architecture [10]. Sensing layer: multi-data sync at ±0.1 ms. Computing layer: fusion, geometric-thermal decoupling, and LSTM 3 ms ahead prediction to generate commands. Execution layer: write commands via FANUC's EPO interface (FOCAS2) synchronized with interpolation cycle, driving servos for real-time correction.

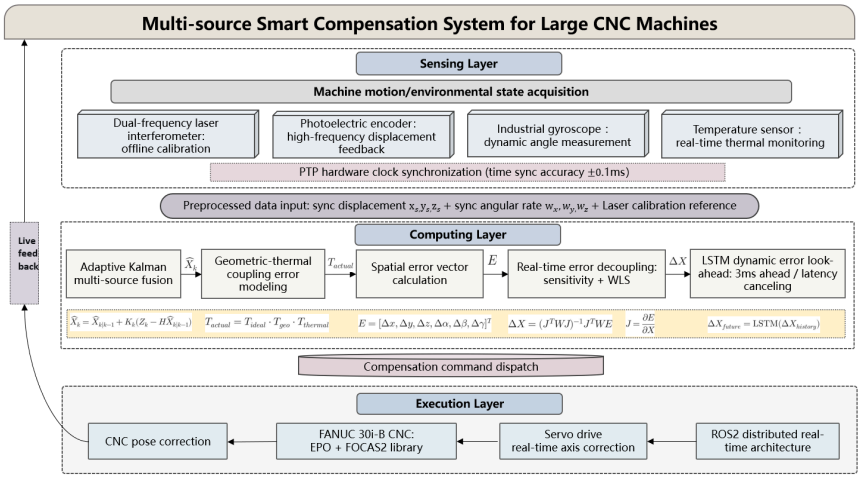


Figure 1. Multi-source fusion intelligent compensation system architecture

3. Geometric–Thermal Error modeling of large-scale CNC machine tools

3.1. HTM-based geometric error optimization model

Based on an XYTZ-type gantry CNC machine tool, a geometric error optimization model incorporating 21 error components—namely geometric errors, Abbe errors, and Bryan errors—is formulated using the Homogeneous Transformation Matrix (HTM) and Multibody System Theory. Under ideal conditions, the ideal homogeneous transformation matrix of each axis is expressed as：

$$H_x = \begin{bmatrix} 1 & 0 & 0 & x \\ 0 & 1 & 0 & 0 \\ 0 & 0 & 1 & 0 \\ 0 & 0 & 0 & 1 \end{bmatrix} H_y = \begin{bmatrix} 1 & 0 & 0 & 0 \\ 0 & 1 & 0 & y \\ 0 & 0 & 1 & 0 \\ 0 & 0 & 0 & 1 \end{bmatrix} H_z = \begin{bmatrix} 1 & 0 & 0 & 0 \\ 0 & 1 & 0 & 0 \\ 0 & 0 & 1 & z \\ 0 & 0 & 0 & 1 \end{bmatrix} \quad (1)$$

Since the transformation matrix on the workpiece side must be inverted to ensure consistency of the reference frame, the ideal overall transformation matrix is expressed as :

DOI: 10.54254/2755-2721/2026.33080

$$H^{ideal} = (H_x)^{-1} \cdot (H_y)^{-1} \cdot \left(H_z\right) \tag{2}$$

Taking the X-axis as an example, following a linear displacement along the axis, the nominal error matrix and the corresponding actual transformation matrices incorporating Abbe and Bryan errors can be formulated based on the HTM, as follows:

$$H_x^a = \begin{bmatrix} 1 & -\varepsilon_{zx} & \varepsilon_{yx} & x+\delta_{xx} \\ \varepsilon_{zx} & 1 & -\varepsilon_{xx} & \delta_{yx} \\ -\varepsilon_{yx} & \varepsilon_{xx} & 1 & \delta_{zx} \\ 0 & 0 & 0 & 1 \end{bmatrix} H_x^{abbe} = \begin{bmatrix} 1 & 0 & 0 & \varepsilon_{zx}L_{yx} - \varepsilon_{yx}L_{zx} \\ 0 & 1 & 0 & -\varepsilon_{xx}L_{zx} + \varepsilon_{zx}L_{xx} \\ 0 & 0 & 1 & 0 \\ 0 & 0 & 0 & 1 \end{bmatrix} H_x^{Bryan}$$

$$= \begin{bmatrix} 1 & 0 & 0 & \varepsilon_{zx}B_{yx} - \varepsilon_{yx}B_{zx} \\ 0 & 1 & 0 & -\varepsilon_{zx}B_{xx} + \varepsilon_{zx}B_{zx} \\ 0 & 0 & 1 & \varepsilon_{yx}B_{xx} - \varepsilon_{zx}B_{yx} \\ 0 & 0 & 0 & 1 \end{bmatrix} \tag{3}$$

Here, ε_{ij} denotes the positioning error along the i-direction induced by the motion of the j-axis; ε_{ij} denotes the roll angular error about the i-axis; L_{ij} and B_{ij} denote the offsets of the Abbe point and Bryan point of the i-axis, respectively, relative to the tool center point in the j-direction; and x, y, and z denote the linear displacements of the respective axes.

Under actual operating conditions, the homogeneous transformation matrix of each axis is formulated as the product of the ideal transformation matrix and the associated error matrix. Taking the X-axis as an example, the actual transformation matrix can be expressed as:

$$H_x^{actual} = H_x^{Bryan} \cdot H_x^{Abbe} \cdot H_x^{e} =$$

$$\begin{bmatrix} 1 & -\varepsilon_{zx} & \varepsilon_{yx} & \varepsilon_{zx}(B_{yx}+L_{yx}) - \varepsilon_{yx}(B_{zx}+L_{zx}) + \delta_{xx} + x \\ \varepsilon_{zx} & 1 & -\varepsilon_{xx} & \varepsilon_{xx}B_{zx} + \varepsilon_{yx}L_{zx} - \varepsilon_{zx}(B_{xx}+L_{yx}) + \delta_{yx} \\ -\varepsilon_{yx} & \varepsilon_{xx} & 1 & \varepsilon_{yx}B_{xx} - \varepsilon_{xx}B_{yx} + \delta_{zx} \\ 0 & 0 & 0 & 1 \end{bmatrix} \tag{4}$$

The actual transformation matrices of the Y-axis and Z-axis follow analogous formulations. Building upon this, Abbe and Bryan error corrections are incorporated, where the corresponding correction matrix is composed of the Abbe offset, the Bryan offset, and angular error components.

For the XYTZ-type machine tool, the X-axis and Y-axis are associated with the workpiece side, and their transformation matrices must be inverted to ensure consistency of the reference frame, whereas the Z-axis is associated with the tool side and is directly multiplied. Consequently, the overall actual homogeneous transformation matrix can be expressed as:

$$H^{actual} = \left(H_x^{actual}\right)^{-1} \cdot \left(H_y^{actual}\right)^{-1} \cdot H_z^{actual} \tag{5}$$

The spatial error vector is defined as the difference between the translational components of the actual pose and the ideal pose:

DOI: 10.54254/2755-2721/2026.33080

$$E_{space} = H^{actual} - H^{ideal} = \begin{bmatrix} E_x \\ E_y \\ E_z \end{bmatrix} \tag{6}$$

This vector captures the coupled effects of all geometric errors and inter-axis perpendicularity errors, thereby serving as a unified input for subsequent error compensation.

3.2. Friction-induced thermal error modeling

During long-stroke continuous machining of large-scale machine tools, friction-induced heating leads to thermal deformation of critical components and variations in refractive index. Accordingly, based on thermal expansion theory, quantitative models of thermal positioning error, thermal straightness error, and thermal angular error are developed, enabling an analytical formulation of thermally induced errors [11].

3.2.1. Modeling of thermal positioning error

Friction-induced heating of the lead screw causes axial thermal elongation. Let α denote the coefficient of thermal expansion of the screw material, ΔT_1 the temperature variation between pre- and post-operation states, and L_1 the effective length of the lead screw. Accordingly, the thermal positioning error is given by:

$$\delta_{ii}(T) = \alpha \cdot \mathrm{c} \cdot L_1 \tag{7}$$

3.2.2. Modeling of thermal straightness error

The temperature gradient between the upper and lower surfaces of the guideway induces bending deformation, thereby degrading the straightness of the motion axis. Let ΔT_2 a denote the temperature difference, L_2 the guideway length, and h the guideway thickness. Accordingly, the thermal straightness error is given by:

$$\delta_{ij}\left(T\right) = \alpha \frac{\Delta T_2 \cdot {L_2}^2}{2h}, \left(\mathrm{i} \neq \mathrm{j}\right) \tag{8}$$

3.2.3. Modeling of thermal angular error

The asymmetric temperature distribution across the column induces tilting, thereby causing angular deviation of the spindle. Let ΔT_3 denote the temperature difference across the column, H the column height, and W the column width. Accordingly, the thermal angular error can be approximated as:

$$\varepsilon_{ij}\left(T\right) = \alpha \frac{\Delta T_3 \cdot H}{W} \tag{9}$$

3.3. Geometric–Thermal Coupling error modeling

To enable unified modeling of static geometric errors and dynamic thermal deformation errors, thermal errors (TE) are incorporated into the geometric error HTM, forming a Geometric–Thermal

DOI: 10.54254/2755-2721/2026.33080

Coupling (GTC) error model. The TE formulations derived in Section 3.2 are first assembled into a TE homogeneous transformation matrix. For a single motion axis, this matrix characterizes the additional pose deviation induced by frictional heating, and is generally expressed as:

$$H_i^{therm} = \begin{bmatrix} 1 & -\varepsilon_{i,z} & -\varepsilon_{i,y} & \delta_{i,x} \\ \varepsilon_{i,z} & 1 & -\varepsilon_{i,x} & \delta_{i,y} \\ -\varepsilon_{i,y} & \varepsilon_{i,x} & 1 & \delta_{i,z} \\ 0 & 0 & 0 & 1 \end{bmatrix}, H^{TE} = H_X^{TE^{-1}} \cdot H_Y^{TE^{-1}} \cdot H_Z^{TE^{-1}} \tag{10}$$

$$H^{GTC} = H^{actual} \cdot H^{TE} \tag{11}$$

4. Multi-source fusion error solution and real-time compensation

4.1. Framework for multi-source fusion error compensation

To meet high-precision real-time compensation needs for multi-source geometric errors in large CNCs, this paper builds a full-process algorithm system from multi-sensor input to three-axis compensation output (Fig. 2). It integrates four core stages: multi-source data synchronization, adaptive Kalman fusion, real-time error decoupling, and LSTM look-ahead prediction with execution, enabling accurate low-latency compensation.

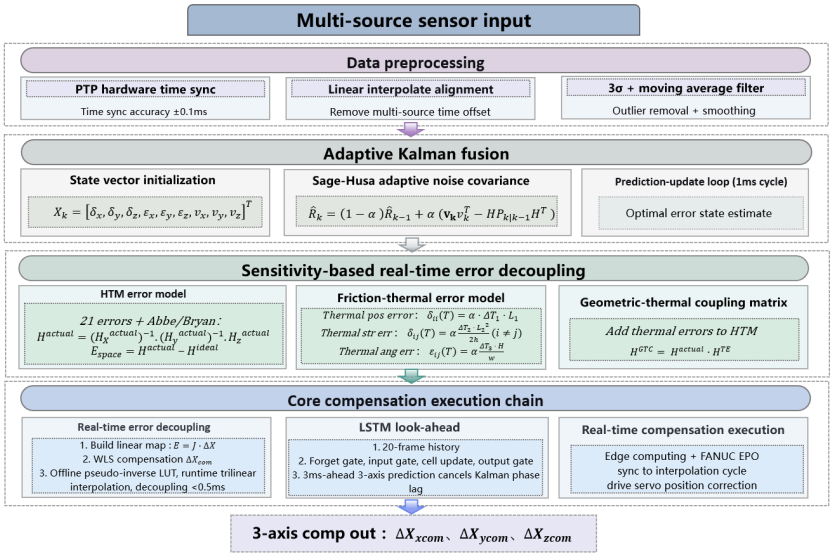


Figure 2. Smart compensation algorithm execution flow

4.2. Multi-source collaborative measurement network

A collaborative "offline calibration + online measurement" network is built using absolute encoders, fiber-optic gyroscopes, and a dual-frequency laser interferometer. Encoders (1 kHz) provide real-time displacement/angle feedback as the main online source. Gyroscopes capture dynamic angular velocity to compensate for encoder lag. The laser interferometer performs offline calibration every 8 hours to correct encoder drift and gyroscope bias.

DOI: 10.54254/2755-2721/2026.33080

4.3. Data preparation and time synchronization

PTP hardware sync (±0.1 ms); linear interpolation aligns async data; 3σ + moving average filter cleans data.

4.4. Adaptive kalman filter fusion

Construct state vector with position, angle, and velocity errors as core:

$$X_k = [\delta_x, \delta_y, \delta_z, \varepsilon_x, \varepsilon_y, \varepsilon_z, \nu_x, \nu_y, \nu_z]^T \tag{12}$$

Estimate observation noise covariance in real time via Sage-Husa adaptive filtering:

$$\widehat{R}_k = \left(1-\alpha\right)\widehat{R}_{k-1} + \alpha\left(\nu_k\nu_k^T - HP_{k|k-1}H^T\right) \tag{13}$$

Where v_k is innovation residual, α (0.95–0.99) residual factor, H observation matrix (sensor-dependent), $P_{k|k-1}$ prediction error covariance. This method adapts to sensor noise online. Through adaptive weighted fusion, a 1 ms prediction-update loop outputs the optimal error state estimate.

4.5. Sensitivity-based decoupling of real-time errors

Build error sensitivity matrix via HTM partial derivatives, establishing linear map

$$E = J \cdot \Delta X \tag{14}$$

Solve compensation ΔX_{com} via weighted least squares. Precompute pseudo-inverse LUT offline; use trilinear interpolation at runtime. Decoupling <0.5 ms.

5. Intelligent compensation strategy and system implementation

5.1. Weighting model for spatial error compensation

In Kalman filtering, the observation noise covariance matrix R reflects the relative confidence of each sensor: a smaller R indicates lower measurement noise and thus a higher fusion weight. The value of R is determined based on the sensor's nominal accuracy and its measured statistical characteristics.

5.2. Lstm-based dynamic error look-ahead prediction

To offset inherent system latency, LSTM is used for dynamic error look-ahead pre-compensation. The sensing layer acquires multi-sensor data; the computing layer performs adaptive Kalman fusion and state estimation, then solves geometric errors via the HTM model. LSTM's four gating mechanisms (forget, input, cell update, output) capture long-term error dynamics. Taking 20 frames of historical errors as input, it outputs 3-axis prediction errors 3 ms ahead, which cancel the Kalman phase lag and keep overall equivalent delay controllable. The FANUC 30i-B system executes the pre-compensation, effectively reducing latency and improving compensation synchronization and accuracy at high speed.

DOI: 10.54254/2755-2721/2026.33080

5.3. Real-time compensation system at millisecond level

To meet real-time demands of high-speed high-precision large CNC machining, the system uses an edge computing platform with PREEMPT_RT real-time kernel and model inference optimization to boost solving efficiency. Based on FANUC 30i-B's EPO (external position offset) and FOCAS2 high-speed library, it achieves μs-level data exchange. PMC window commands build a compensation write channel synchronized with the CNC interpolation cycle, adding three-axis compensation values to position commands in real time without system restart. This scheme delivers closed-loop compensation with ≤1.5 ms end-to-end delay and completes end-to-end deterministic communication adaptation with the ROS2 distributed real-time architecture.

6. Conclusion

This paper addresses the core pain points of large CNC long-stroke machining—offline geometric error lag, difficult multi-source decoupling, and insufficient real-time compensation—by proposing a multi-source fusion online measurement and intelligent compensation system. A geometric-thermal coupled 21-error model, adaptive Kalman fusion, LSTM look-ahead, and decoupling compensation architecture are built to achieve high-precision closed-loop compensation. System design and analysis show that over a 5 m stroke, the expected spatial error compensation accuracy is better than ±10 μm, a reduction of over 60% compared to pre-compensation, with theoretical stability under complex conditions.

References

[1] Sun, G. M., Han, B., Zhang, D. W., et al. Research Progress on Spatial Error Modeling and Identification Methods for CNC Machine Tools Oriented Towards Error Compensation [J/OL]. Journal of Mechanical Engineering, 1-27 [2025-07-30].
[2] Huang, M. X., Niu, X. H., Niu, J. Q., et al. Geometric Error Analysis and Modeling of Three-Axis CNC Machine Tools [J]. Journal of Tianjin University of Technology, 2024, 40(01): 22-29.
[3] Chen, Q. H., Guan, Y., Zhou, S., et al. High-Precision Wave Plate Measurement Based on Dual-Frequency Laser Interferometric Phase Detection [J]. Acta Optica Sinica, 2023, 43(01): 110-116.
[4] Zhang, C. Research on Online Measurement and Active Compensation Technology for Geometric Errors of Large-Scale Machine Tools [D]. Tianjin University, 2022.
[5] Huang, Y. B., Fan, K. C., Lou, Z. F., & Sun, W. (2020). A novel modeling of volumetric errors of three-axis machine tools based on Abbe and Bryan principles. International Journal of Machine Tools and Manufacture, (), 103527–.
[6] Limaverde Filho, J. O. A., Fortaleza, E. L. F., Silva, J. G., et al. Adaptive Kalman filtering for closed-loop systems based on the observation vector covariance [J]. International Journal of Control, 2022, 95(7): 1731-1746.
[7] Liang, J. P., Zhu, S. Y., Zhang, N., et al. Downscaling of WRF-Predicted Air Temperature Based on Machine Learning and Adaptive Kalman Filter: A Case Study in Chongli, Hebei Province [J]. Transactions of Atmospheric Sciences, 2025, 48(03): 463-475.
[8] Luo, Y., Gao, J., Chen, D., Zhang, L., Liu, Y., & Zhong, Y. (2024). Accurate error compensation method for multi-axis parallel machine via singularized jacobi geometric parameter correction and coupling error evaluation. Robotics and Computer-Integrated Manufacturing, 89, 102771.
[9] Ji, S., Ni, H., Hu, T., Sun, J., Yu, H., & Jin, H. (2024). DT-CEPA: A digital twin-driven contour error prediction approach for machine tools based on hybrid modeling and sparse time series. Robotics and Computer-Integrated Manufacturing, 88, 102738.
[10] Levinson, J., Askeland, J., Becker, J., et al. Towards fully autonomous driving: Systems and algorithms [C]//2011 IEEE Intelligent Vehicles Symposium (IV). IEEE, 2011: 163-168.
[11] Ma, C., Li, M. M., Liu, J. L., et al. Research on the Application of Thermal Error Compensation in Digital Twin Systems [J]. Journal of Harbin University of Science and Technology, 2025, 30(01): 129-137.